ELSEVIER

Journal of Power Sources 77 (1999) 74–82

JOURNAL OF POWER SOURCES

Analysis of the discharge performance of a flooded lead/acid cell using mathematical modelling

Sung Chul Kim, Won Hi Hong *

Department of Chemical Engineering, Korea Advanced Institute of Science and Technology, 373-1 Kusung-dong, Yusung-gu, Taejeon 305-701, South Korea

Received 28 August 1998; accepted 22 October 1998

Abstract

The discharge performance of the flooded lead/acid cell has been modelled. The model takes account of the diffusion–precipitation mechanism in the negative electrode. The effect of the dissolution of lead, the diffusion of lead ions and the precipitation of lead sulfate crystals is not even neglected at low current discharge and is increased as the discharge current increases. The discharge curves predicted by the model are in good agreement with the experimental data. © 1999 Elsevier Science S.A. All rights reserved.

Keywords: Lead acid cell; Discharge; Porous electrode; Modelling

1. Introduction

Improvement in the performance of the lead/acid batteries is achieved by proper selection of materials, optimization of the manufacturing process, and development of the electrode design. Mathematical modelling of the lead/acid cell is needed to investigate the performance of the batteries as well as the influence of the materials selected or made. An appropriate model provides information that is not obtained from tests and allows the optimum design of battery.

The two main mathematical approaches to describe the behaviour of the batteries are the resistive grid model and the macroscopic homogeneous model. The former is used to study current and overpotential distributions along the electrode surface by dividing the battery electrode into a discrete number of elements with independent physical and electrochemical properties. The latter is used to develop the electrode kinetics and the transport equations in order to investigate the cell behaviour.

Maia et al. [1] have examined the behaviour of the electrode at high and low discharge current, using the resistive grid model. This model can be used to obtain the current and ohmic overpotential distributions along the electrode, but it did not provide any information about variation in the porosity, the distribution of the electrolyte, and the effect of the separator. Newman and Tiedemann [2] first developed the macroscopic homogeneous model and simulated the discharge performance of the lead/acid battery. Gu et al. [3] observed variations of the electrolyte concentration, porosity and reaction rates during discharge, charge and rest. The effect of acid stratification is demonstrated to predict transient behaviour of lead/acid batteries by Gu et al. [4]. All these studies examined only the charge transfer in the negative electrode and did not consider the solid-state reaction.

For valve-regulated lead/acid batteries, Landfors et al. [5] compared experimental data with numerically predicted results by taking account of the influence of the grid. Bernardi and Carpenter [6] developed a mathematical model of lead/acid batteries by adding the oxygen recombination reaction. Nguyen et al. [7] presented a model analogous to the flooded type and examined the dynamic behaviour of the cell during discharge with respect to cold cranking amperage and reserve capacity.

Ekdunge et al. [8] and Ekdunge and Simonsson [9,10] have studied the influence of organic expander on the recharge kinetics and structural changes in the lead electrode and derived a mathematical model which took into consideration the diffusion–precipitation mechanism. Unfortunately, the effects of the positive electrode and the separator were not considered.

* Corresponding author

PII: S0378-7753(98)00175-X

The approach presented here is based on the model given by Gu et al. [3] and incorporates the diffusion–precipitation mechanism studied by Ekdunge and Simonsson [9] in the reaction kinetics of the negative electrode. Experimental data are obtained and compared with the results of our model and that of Gu et al. [3] in order to analyze the discharge behaviour of the flooded lead acid cell.

2. Mathematical model

2.1. Description of model

The kinetic behaviour of a lead electrode in the lead/acid battery during discharge has been presented by Ekdunge and Simonsson [9] and the transfer current, j, is written as follows (the dependence of the electrolyte concentration is included):

$$j = ai_{\mathrm{o,ref}}\left(\frac{c}{c_{\mathrm{ref}}}\right)^{\gamma}\frac{1-\exp\left[\left(\alpha_{\mathrm{a}}+\alpha_{\mathrm{c}}\right)\dfrac{F\eta}{RT}\right]}{\dfrac{ai_{\mathrm{o,ref}}}{j_{\mathrm{lim}}}-\exp\left[\alpha_{\mathrm{c}}\dfrac{F\eta}{RT}\right]} \tag{1}$$

where a denotes active surface area of the electrode; c is the concentration of the binary electrolyte; c_{ref} is the reference concentration of the binary electrolyte; $i_{\mathrm{o,ref}}$ is the exchange-current density at $c = c_{\mathrm{ref}}$; η is the total local overpotential with respect to the equilibrium potential; γ is the exponent for the concentration dependence.

The limiting current density, j_{lim}, affects significantly the polarization curves and is determined by the dissolution rate of lead, the diffusion rate of lead ions and the precipi-tation rate of lead sulfate crystals. The transfer-current density of the positive electrode can be obtained by the Butler–Volmer equation.

The model is based on the assumptions made by Tiedemann and Newman [11], as follows.

(i) The lead acid/cell comprises a lead dioxide electrode (PbO_2), an electrolyte reservoir, a porous separator and a lead electrode (Pb).

(ii) It is assumed that sulfuric acid is completely dissociated into H^+ and HSO_4^- ions.

(iii) The model is one-dimensional in the direction perpendicular to the plane of the electrodes.

(iv) Porous electrodes are assumed to be macro-homogeneous.

(v) The cell is considered to be isothermal during its operation.

The volume-average technique presented by Vidts and White [12] is used to develop the model.

During discharge, the following electrochemical reactions occur in the positive and negative electrode.

Positive electrode:

$$PbO_2(s) + HSO_4^- + 3H^+ + 2e^- \rightarrow PbSO_4(s) + 2H_2O \tag{I}$$

Negative electrode:

$$Pb(s) + HSO_4^- \rightarrow PbSO_4(s) + 2e^- + H^+ \tag{II}$$

The variation in porosity during discharge can be express as:

$$\frac{\partial \varepsilon}{\partial t} = \frac{1}{2F}a_1 j \tag{2}$$

where the coefficient a_1 is given in Table 1.

There are no changes of porosity in the reservoir and the separator, i.e.,

$$\varepsilon = 1 \quad \text{for the reservoir, and} \tag{3}$$

$$\varepsilon = \varepsilon_{\mathrm{sep}} \quad \text{for the separator.} \tag{4}$$

The total current density, i, is the sum of the current density in the solid phase, i_1, and the current density in the conducting liquid phase i_2, i.e.,

$$i = i_1 + i_2. \tag{5}$$

For the solid phase, the current density in the solid phase i_1 follows Ohm's law, viz.,

$$i_1 = \sigma * \nabla\phi_1 \tag{6}$$

where the effective conductivity of the solid matrix $\sigma *$ is defined in Table 1. In fact, σ represents the conductivity of the electrode solid phase and exm1, exm4 are empirically determined constants for the tortuosity of the solid matrix.

Table 1
Coefficients and effective properties used in model equations

	Positive electrode	Reservoir	Separator	Negative electrode
a_1	$(MW_{PbSO_4}/\rho_{PbSO_4}) - (MW_{PbO_2}/\rho_{PbO_2})$	–	–	$(MW_{Pb}/\rho_{Pb}) - (MW_{PbSO_4}/\rho_{PbSO_4})$
a_2	$3 - 2t_+^0$	0	0	$1 - 2t_+^0$
$\sigma *$	$\sigma_{PbO_2}\varepsilon^{exm1}$	–	–	$\sigma_{Pb}\varepsilon^{exm4}$
$k *$	$\kappa\varepsilon^{ex1}$	–	–	$\kappa\varepsilon^{ex4}$
$D *$	$D\varepsilon^{ex1}$	0	$D\varepsilon_{sep}^{ex3}$	$D\varepsilon^{ex4}$

The current density in the electrolytic solution is proportional not only to the concentration gradient but also to the electric potential gradient, i.e.,

$$i_2 = -\kappa * \nabla\phi_2 - \kappa^{**}\nabla(\ln c) \tag{7}$$

where the effective conductivity $k*$ is given in Table 1 and $k**$ is expressed as:

$$\kappa^{**} = \frac{RT\kappa *}{F}(2t_+^0 - 1). \tag{8}$$

In this case, κ denotes the electrolyte conductivity and ex1, ex4 are exponents in the effective property. The transference number of the positive ion, t_+^0, is defined relative to the solvent.

Since there is no solid electrode in the reservoir and the separator, the potential in the solid phase equals zero, i.e.,

$$\phi_1 = 0. \tag{9}$$

The material balance for the acid concentration in the liquid phase becomes

$$\frac{\partial(\varepsilon c)}{\partial t} + v * \nabla c = \nabla \cdot (D * \nabla c) + \frac{a_2 j}{2F} \tag{10}$$

where the coefficient a_2 and the effective diffusivity $D*$ are denoted in Table 1.

The volume-average velocity $v*$ is used as the reference velocity [12]. The current density of liquid phase in the positive and negative electrode, respectively, is related to the charge leaving the solid matrix and is determined by the electrochemical kinetic reactions which occur at the interface between the active material and the electrolyte inside electrode.

From the conservation of charge, the electroneutrality condition is applied to Eq. (5)

$$\nabla i_1 + \nabla i_2 = 0 \tag{11}$$

so that

$$\nabla i_1 = -\nabla i_2 = j. \tag{12}$$

The Butler–Volmer equation is used to express the overall electrode reaction rate, j, in the positive electrode:

$$j = ai_{o1,ref}\left(\frac{c}{c_{ref}}\right)^{\gamma}\left[\exp\left(\alpha_{a1}\frac{F\eta}{RT}\right) - \exp\left(\alpha_{c1}\frac{F\eta}{RT}\right)\right]. \tag{13}$$

The overall electrode reaction rate, j, at the negative electrode is suggested by Eq. (1), which takes account of the diffusion–precipitation mechanism as well as the dependence of the electrolyte concentration, i.e.,

$$j = ai_{o4,ref}\left(\frac{c}{c_{ref}}\right)^{\gamma}\frac{1 - \exp\left[(\alpha_{a4} + \alpha_{c4})\frac{F\eta}{RT}\right]}{\frac{ai_{o4,ref}}{j_{lim}} - \exp\left[\alpha_{c4}\frac{F\eta}{RT}\right]}. \tag{14}$$

The overpotential η is defined as

$$\eta = \phi_1 - \phi_2 - U_{PbO_2} \tag{15}$$

for the positive electrode, and

$$\eta = \phi_1 - \phi_2 \tag{16}$$

for the negative electrode. The equilibrium potential U_{PbO_2} is evaluated at a reference concentration c_{ref}. The electroactive surface area a is related to the state-of-discharge and is given by [13]:

$$a = a_{max*}\left(\frac{Q}{Q_{max}}\right)^{\zeta} \tag{17}$$

where Q is the charge density in the electrode; Q_{max} is the theoretical maximum capacity; ζ is the exponent for charge dependence of the specific electroactive area.

The unknowns in each region are the potential in the solid phase ϕ_1, the potential in the liquid phase ϕ_2, the electrolyte concentration c, the porosity ε, and the current density in the liquid phase i_2. In order to solve the governing equations derived earlier for each region, initial and boundary conditions are necessary.

2.2. Initial conditions

The initial values for electrolyte concentration and porosity are as follows

$$c = c_{ref} \tag{18}$$

for all x,

$$\varepsilon = \varepsilon_{PbO_{2,max}} \tag{19}$$

for the positive electrode, and

$$\varepsilon = \varepsilon_{Pb,max} \tag{20}$$

for the negative electrode. The initial potential distribution should be calculated from the equation for electrode kinetic reaction.

2.3. Boundary conditions

2.3.1. At centres of positive and negative electrodes

From the conditions of symmetry and zero-flux, these yield:

$$\nabla c = 0 \tag{21}$$

$$\nabla\varepsilon = 0 \tag{22}$$

$$\nabla\phi_2 = 0. \tag{23}$$

There is no electrolyte at these boundaries, i.e.,

$$i_2 = 0. \tag{24}$$

At the center of the positive electrode, the potential on the surface of the current-collector is taken to be zero, i.e.,

$$\phi_1 = 0. \tag{25}$$

In order to calculate the potential of the solid phase, Eq. (14) is used to described the centre of the negative electrode.

Table 2
Parameters used in calculations

Parameter	Value	References
Positive electrode		
Half thickness of plate	0.09 cm	measured
Maximum charge state	2620 C cm^{-3}	[7]
Discharge reaction parameter ($a_{max1} i_{o1,ref}$)	0.073 A cm^{-3}	[7]
α_{a1}	1.15	[7]
α_{c1}	0.85	[7]
$\gamma 1$	1.5	[3]
$\zeta 1$	1.0	[3]
Lead dioxide conductivity	500 S cm^{-1}	[6]
ex1	1.5	[7]
exm1	0.5	[7]
Negative electrode		
Half thickness of plate	0.07 cm	measured
Maximum charge state	3120 C cm^{-3}	[7]
Discharge reaction parameter ($a_{max4} i_{o4,ref}$)	0.11 A cm^{-3}	[7]
α_{a4}	1.55	[7]
α_{c4}	0.45	[7]
$\gamma 4$	1.5	[3]
$\zeta 4$	1.0	[3]
Lead conductivity	1.8×10^4 S cm^{-1}	[6]
ex4	1.5	[7]
exm4	0.5	[7]
Reservoir		
Thickness of reservoir	0.07 cm	measured
Separator		
Thickness of separator	0.022 cm	measured
Porosity	0.60	measured
ex3	1.50	[6]
Electrolyte		
Acid concentration	4.9×10^{-3} mol cm^{-3}	measured
Transference number	0.72	[11]
Partial molar volume of acid	45 cm^3 mol^{-1}	[11]

2.3.2. At the positive electrode solidus reservoir, reservoir solidus separator and separator solidus negative electrode interfaces

The flux of the electrolyte and the current density in the liquid phase are continuous, i.e.,

$$\varepsilon * \nabla c|_+ = \nabla c|_{res} \quad (26)$$

$$\varepsilon * \nabla \phi_2|_+ = \nabla \phi_2|_{res} \quad (27)$$

$$\varepsilon * \nabla c|_{sep} = \varepsilon * \nabla c|_- \quad (28)$$

$$\varepsilon * \nabla \phi_2|_{sep} = \varepsilon * \nabla \phi_2|_- \quad (29)$$

$$D\nabla c - cv *|_{res} = D * \nabla c - cv *|_{sep} \quad (30)$$

where the vertical bar signifies that the derivative and coefficients are evaluated in the region designated by the bar subscript.

All the current flows through the liquid phase, because there is no solid electrode in these boundaries.

$$i_2 = i \quad (31)$$

$$\nabla \phi_1 = 0. \quad (32)$$

The variation of the porosity is determined by the conversion of the active material in the electrode, namely:

$$\frac{\partial \varepsilon}{\partial t} = \frac{1}{2F} a_1 j. \quad (33)$$

At the interface between the reservoir and the separator, the porosity is constant.

$$\varepsilon = \varepsilon_{sep} \quad (34)$$

2.4. Numerical procedure

The above equations are discretized by the method of finite differences with accuracy of the square of the node spacing. The time derivatives are formulated by means of the Crank–Nicolson method. The non-linear multi-region problems are solved by the Newton–Raphson iterative method [14] and MBAND presented by Fan and White [15].

2.5. Parameters

The material properties and the cell parameters used in the simulation are presented in Table 2. The diffusion coefficient, D, and the electrolyte conductivity, κ, which are considered to be dependent on temperature as well as concentration, are given by Tiedemann and Newman [11] as follows:

$$D = \exp\left[\frac{2174.0}{298.15} - \frac{2174.0}{T}\right](1.75 + 260.0c) \times 10^{-5} \quad (35)$$

$$\kappa = c\exp\left[1.1104 + (199.475 - 16\,097.781c)c + \frac{3916.95 - 99\,406.0c - \frac{721\,860}{T}}{T}\right]. \quad (36)$$

3. Experimental

The experimental apparatus comprised a test cell in a water bath and charge–discharge equipment connected to a personal computer. Electrodes from automotive batteries were used in the experiment and were provided by Korea Storage Battery, Ltd. The dimensions of the positive electrode were: 125.5 mm (height) × 143 mm (width) × 1.8 mm (thickness). The negative electrode had the same height and width but a reduced thickness of 1.4 mm. The separator was an envelope type prepared by DARAMIC, Inc. The cell stack was composed of five positive electrodes and six negative electrodes and the case of the cell was made of polycarbonate. After construction of the cell stack, sulfuric acid of 4.9 M (1.280 relative density at 25°C) was poured into the cell. The cell was placed in a circulator at 25°C for 2 h to allow the sulfuric acid to soak into the electrodes. The terminals of the cell were connected to the discharge equipment (UBT, Digatron) and the test cell was charged for 2 h with 2.8 mA cm^{-2} before the discharge test. All experiments were performed at 25°C. The discharge current density was between 1.7 and 33.6 mA cm^{-2} and the cut-off voltage was varied from 1.6 to 1.75 V $cell^{-1}$ according to the discharge current. The charge current density was 3.3 mA cm^{-2} and the cell was recharged corresponding to 130 to 150% of the discharge capacity. After recharge, the cell was placed in a circulator for 3 to 5 h and then the next discharge experiment was performed.

4. Results and discussion

The discharge performance of the flooded lead/acid cell is investigated to validate our model by comparing the experimental data with theoretically predicted values. The limiting current density, j_{lim}, used in our study was not measured and was chosen as a fitting parameter for experimental curves. The discharge behaviour of the cell has been measured and compared with simulation results. Investigation has also been made of the limiting current density to discharge current during discharge, the numerically predicted profile of the electrolyte concentration in the cell during discharge and the rest period, and the effect of cell parameters on cell behaviour.

4.1. Comparison of models with experiment

The result of a discharge experiment at 33.6 mA cm^{-2} is shown in Fig. 1. The slight initial rise in the cell voltage is the 'voltage-dip' which is due to the formation of lead sulfate crystals [3,16], but it is not considered in our model. It depends on the concentration of ions and the presence of inhibitors. The values predicted by Gu et al. [3] are higher than the experimental data and decrease sharply near the end of discharge. The cut-off voltage is 1.60 V $cell^{-1}$. The discharge time calculated by Gu et al. [3] and by our model differs very little from the experimental value. In our model the limiting current density, j_{lim}, is taken to be -1×10^{-3} A cm^{-3}. It should be mentioned, however, that the extent of the dissolution of lead, the diffusion of lead ions and the precipitation of lead sulfate crystals all affect greatly the polarization of the negative electrode. If the limiting current density, $-j_{lim}$, is much higher than $ai_{o,ref}$, that is, the dissolution rate of the lead, the diffusion rate of lead ions and the precipitation rate of lead sulfate crystals are much faster than the charge-transfer reaction, then the results of our model are the same as those of Gu et al. [3].

Reserve-capacity performance is shown in Fig. 2. The test is carried out at 25°C with a discharge current of 14.0 mA cm^{-2} and the cell voltage is measured. The initial voltage drop in experimental data is not quite different

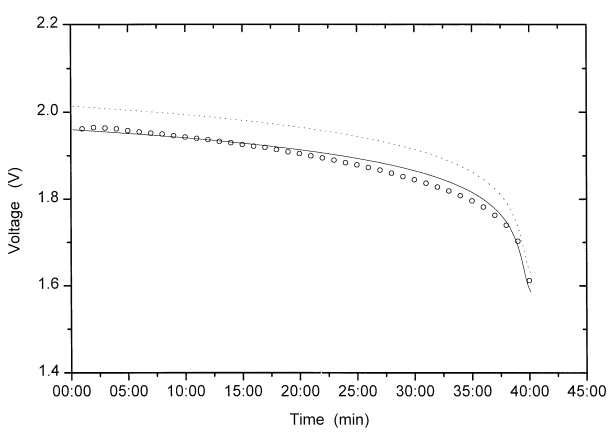

Fig. 1. Comparison of theoretically predicted and measured cell voltage at a discharge of 33.6 mA cm^{-2} (○: experimental data, ···: Gu et al. [3], ————: this work with $j_{lim} = -1\times10^{-3}$ A cm^{-3}).

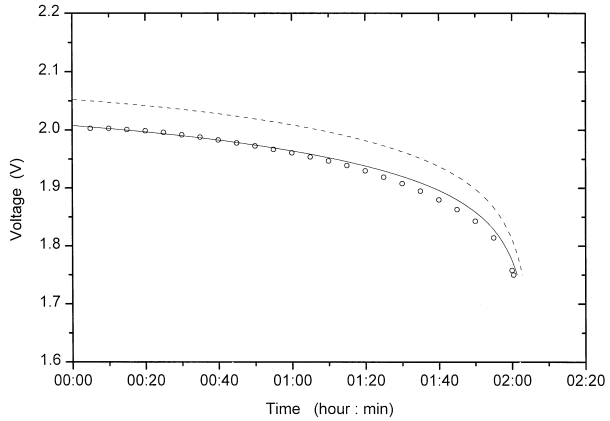

Fig. 2. Comparison of theoretically predicted and measured cell voltage at a discharge of 14.0 mA cm^{-2} (○: experimental data, ---: Gu et al. [3], ————: this work with $j_{lim} = -2 \times 10^{-3}$ A cm^{-3}).

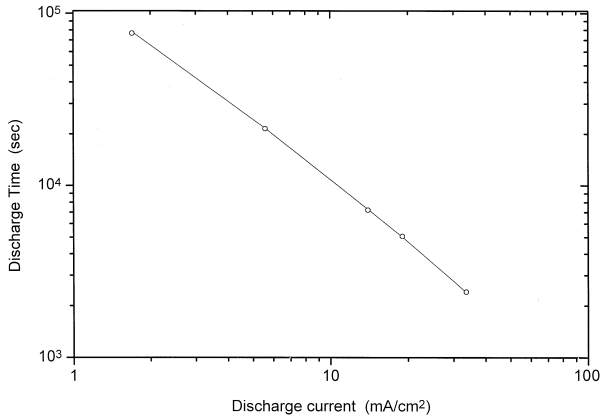

Fig. 4. Discharge time vs. discharge current (○: experimental data, ————: this work).

from our model, but after 1 h the voltage drop simulated by our study is lower than the experimental result. The model of Gu et al. [3], reports an initial voltage drop that is 0.047 V higher than the experimental data and the slope of the voltage drop becomes steeper near the end of discharge. The limiting current density used in our study is taken to be -2×10^{-3} A cm^{-3}. The reaction term in the negative electrode is also not discarded.

The cell behaviour for a discharge of 5.6 mA cm^{-2} is shown in Fig. 3. The cell voltage simulated by our model is higher than the experimental data during the initial stage, but is just about the same as the experimental results near the end of discharge. The curve simulated by the model of Gu et al. [3] lie above the experimental data. It is shown that the cell voltage decreases sharply near the end of discharge in the results of Gu et al. [3]. The limiting current density is assigned as -3×10^{-3} A cm^{-3} in our study.

The increase in the initial voltage drop with increasing discharge current is obvious in the discharge current–voltage plots. The cell voltage is determined by the ohmic resistances and the polarization effects. When the cell is discharged, the potential deviates from the equilibrium value. This indicates that the effects of polarization developed around the electrodes are increased. When the discharge current is increased, the polarization is increased. As the discharge current is higher, the active material in the outermost layer of the electrode becomes more deactivated at a low degree of discharge [5].

When the discharge current is constant, the slope of the voltage–time plot denotes the drop in cell voltage. This value is determined by utilization of the electrolyte and the reaction area. As the porosity of the electrodes is increased, the ohmic losses are reduced and the effective diffusivity is increased. The behavior of the positive electrode controls the cell performance under high-current discharge. Ohmic losses in the negative electrode are smaller than in the positive, which is due to the higher conductivity of the negative active-material [1]. The active-material utilization is affected not only by the electrolyte but also by the local current density. At the end of discharge, a rapid increase in the ionic resistance through the electrode causes the cell behaviour to be limited by plugging of the entrances of the electrode.

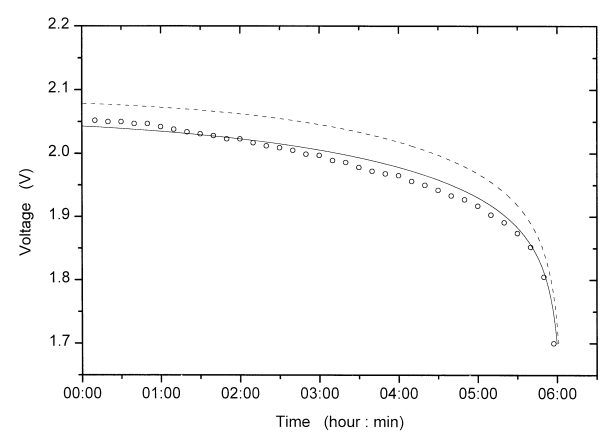

Fig. 3. Comparison of theoretically predicted and measured cell voltage at a discharge of 5.6 mA cm^{-2} (○: experimental data, ---: Gu et al. [3], ————: this work with $j_{lim} = -3 \times 10^{-3}$ A cm^{-3}).

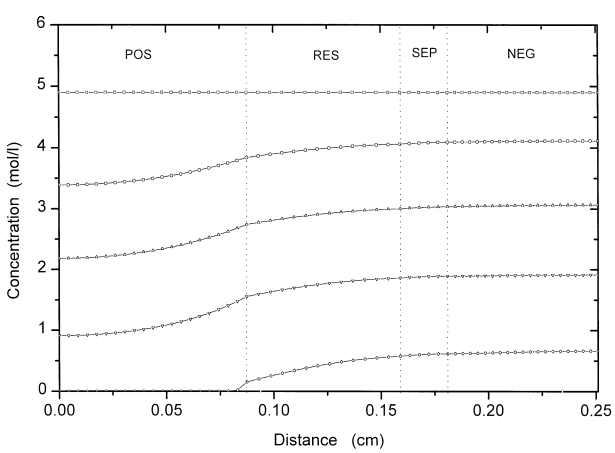

Fig. 5. Predicted profiles of acid concentration at a discharge of 33.6 mA cm^{-2} (– □ –: initial, – ∘ –: 10 min, – △ –: 20 min, – ▽ –: 30 min, –◇–: at the end of discharge).

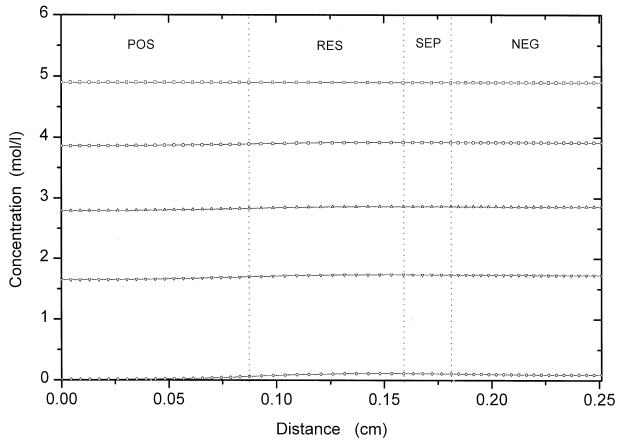

Fig. 6. Predicted profiles of acid concentration at a discharge of 1.7 mA cm^{-2} (– □ –: initial, – ∘ –: 5 h, – △ –: 10 h, – ▽ –: 15 h, –◇–: at the end of discharge).

The discharge current vs. discharge time is demonstrated in Fig. 4. The numerical prediction by our model is good agreement with the experimental result.

4.2. Concentration profile during discharge and rest

The concentration profiles in the cell during discharge are displayed in Fig. 5, when the discharge current is varied from high to low. The initial concentration of the electrolyte is 4.9 mol^{-1} (1.280 relative density at 25°C). In Fig. 5, the change in the electrolyte concentration is shown for $t = 10$, 20, and 30 min to a cut-off voltage with the same condition used in Fig. 1. The electrolyte concentration profiles in Fig. 6 are displayed for $t = 5$, 10, and 15 h with a low discharge current of 1.7 mA cm^{-2}. It can be seen that the concentration gradients and the mass transfer resistance between the reservoir and the positive electrode become higher as the discharge current is set from low to high. The discharge of the cell is ended by acid depletion in the positive electrode, which comes from the transfer

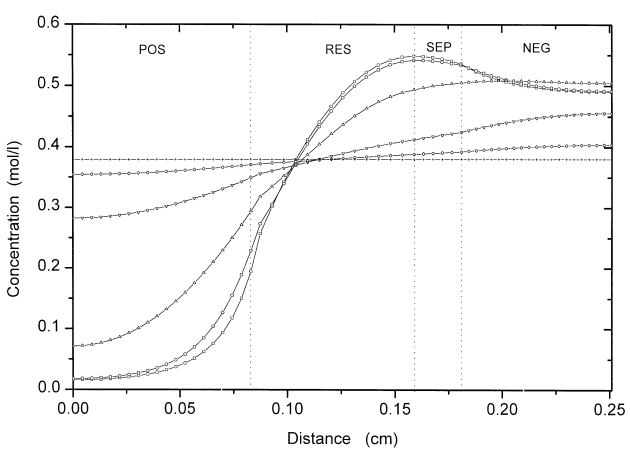

Fig. 7. Predicted profiles of acid concentration distribution during rest (– □ –: at the end of discharge with 14.0 mA cm^{-2}, – ∘ –: 10 s, – △ –: 100 s, – ▽ –: 500 s, –◇–: 1000 s, – + –: 2545 s).

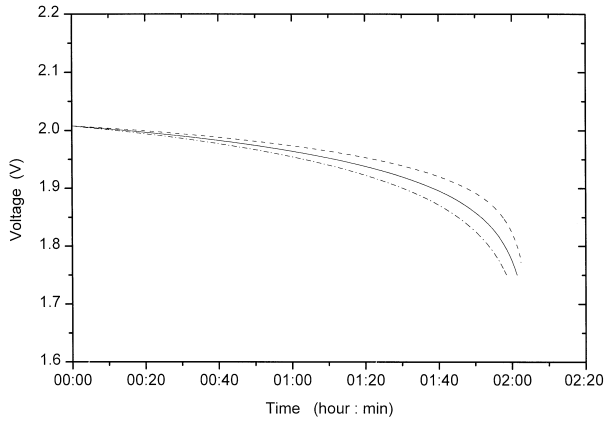

Fig. 8. Effect of cell parameter on discharge behaviour with 14.0 mA cm^{-2} for ---: $\gamma = 1.0$, ————: $\gamma = 1.5$, – · –: $\gamma = 2.0$.

resistance of the electrolyte migration [3,5]. The cell behaviour during the rest period is simulated in Fig. 7, after the cell has been discharged with 14.0 mA cm^{-2} to the cut-off voltage. The initial profile represents the electrolyte concentration at the end of discharge. To develop a new equilibrium state, it takes about 2545 s after the end of discharge.

4.3. Effect of parameters on cell behaviour

The effect of the parameters on the cell performance is investigated by using numerical simulation. As the porosity in the positive or negative electrode is reduced, ohmic losses are increased and the effective diffusivity and conductivity are decreased [3]. Consequently, the discharge capacity drops rapidly. The exchange current density, i_o, has a great impact on the initial voltage drop [17]. The voltage drop increases with increasing reaction order, γ, as in Fig. 8, because it affects the dependence of the electrolyte concentration. The voltage drop is found to be more sensitive to the cathodic transfer coefficient, α_c. For example, in Fig. 9, as α_c in the positive electrode is increased, the slope of the voltage drop is decreased.

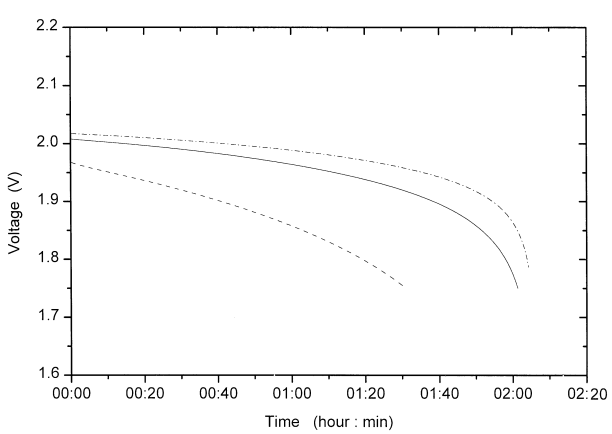

Fig. 9. Effect of cell parameter on discharge behaviour with 14.0 mA cm^{-2} for ---: $\alpha_c = 0.3$, ————: $\alpha_c = 0.85$, – · – ·: $\alpha_c = 1.5$.

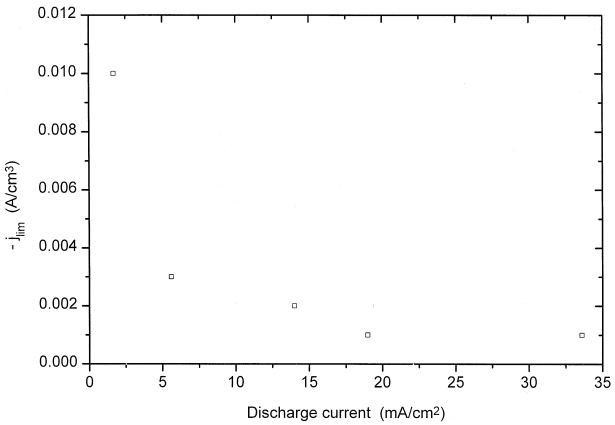

Fig. 10. Limiting current density ($-j_{\text{lim}}$) vs. discharge current.

4.4. Limiting current density

The limiting current density is determined by the influence of the diffusion of lead ions from an electroactive lead surface to a growth site on a lead sulfate crystal and/or by the kinetics of precipitation of lead sulfate [8,17]. The values of the limiting current density as a function of the discharge current density is shown in Fig. 10. The value of j_{lim} is -1×10^{-2} A cm^{-3} at a low rate of discharge and -1×10^{-3} A cm^{-3} at a high rate of discharge. The limiting current density, $-j_{\text{lim}}$, decreases with increasing discharge current. At high rates of discharge, the deactivated layer is formed at the outermost of the electrode and affects the electrode kinetic reactions. As $-j_{\text{lim}}$ is decreased, the active-mass utilization becomes lower and the voltage drops rapidly. The electrode reaction rates are lower than the charge transfer reactions, that is, lead ions are slowly converted to lead sulfate crystals.

5. Conclusions

The discharge behaviour of the flooded lead/acid cell has been investigated to validate the model by comparing the experimental data with numerically predicted results. Consideration has been to the diffusion–precipitation mechanism in the negative electrode during discharge. The cell voltage vs. time, the concentration profiles during discharge and rest, and the discharge time vs. discharge current have been presented. The results of applying our model to analyze the experimental data can be summarized as follows.

(i) When the discharge current is high, the concentration gradient in the cell becomes steeper and the transfer resistance of the electrolyte migration is increased. The behaviour of the positive electrode controls the cell performance at high rates of discharge.

(ii) The value of $-j_{\text{lim}}$ decreases with increasing discharge current. Although the discharge current is low, the electrode kinetic reaction in the negative of the diffusion of lead ions and the precipitation of lead sulfate cannot be discarded.

(iii) As $-j_{\text{lim}}$ is decreases, the active-mass utilization is lowered and the electrode reaction rate is slower than the charge-transfer reaction.

6. Symbols

a	active surface area of the electrode (cm^2 cm^{-3})
$a_{\max}$	maximum specific active surface area of the electrode (cm^2 cm^{-3})
c	concentration of the binary electrolyte (mol cm^{-3})
c_{ref}	reference concentration of the binary electrolyte (mol cm^{-3})
D	diffusion coefficient of the binary electrolyte (cm^2 s^{-1})
ex	exponents on porosity
exm	empirically determined constant for tortuosity of the solid matrix
F	Faraday's constant (96,487 C mol^{-1})
$i_{\text{o,ref}}$	exchange current density at c_{ref} (A cm^{-2})
i	total applied current density based on projected electrode area (A cm^{-2})
i_1	current density in the solid phase (A cm^{-2})
i_2	current density in the conducting liquid phase (A cm^{-2})
j	reaction current per unit volume of electrode (A cm^{-3})
j_{lim}	limiting current density for the negative electrode (A cm^{-3})
MW_i	molecular weight of species i (g mol^{-1})
Q	charge density in the electrode
$Q_{\max}$	theoretical maximum capacity (C cm^{-3})
R	universal gas constant (8.3143 J mol^{-1} K)
t	time (s)
t_{o}^{+}	transference number of H^+ with respect to the solvent velocity
T	absolute temperature (K)
U_{PbO_2}	equilibrium potential at c_{ref} for positive electrode (V)
$v*$	volume-average velocity (cm s^{-1})
x	distance from the center of the positive electrode (cm)

Greek letters

α_{a}	anodic transfer coefficient for electrode
α_{c}	cathodic transfer coefficient for electrode
γ	exponents for the concentration dependence of the exchange current density
ε	porosity
ε_{sep}	porosity of the separator
$\varepsilon_{\max}$	porosity at fully charged state of the electrodes
ζ	exponents for the charge dependence of the specific active surface area
κ	electrolyte conductivity (S cm^{-1})

ρ_i	density of species i (g cm^{-3})
σ_i	conductivity of the electrode solid phase (S cm^{-1})
ϕ_1	potential in the electrode matrix (V)
ϕ_2	potential in the solution (V)
η	total local overpotential with respect to the equilibrium potential

Subscripts

+	positive electrode
−	negative electrode
res	reservoir
sep	separator

Acknowledgements

The authors wish to thank Korea Storage Battery, Ltd. for financial support of this work.

References

[1] G. Maia, E.A. Ticianelli, E.R. Gonzalez, J. Appl. Electrochem. 23 (1993) 1151.
[2] J. Newman, W. Tiedemann, AIChE J. 21 (1975) 25.
[3] H. Gu, T.V. Nguyen, R.E. White, J. Electrochem. Soc. 134 (1987) 2953.
[4] W.B. Gu, C.Y. Wang, B.Y. Liaw, J. Electrochem. Soc. 144 (1997) 2053.
[5] J. Landfors, D. Simonsson, A. Sokirko, J. Power Sources 55 (1995) 217.
[6] D.M. Bernardi, M.K. Carpenter, J. Electrochem. Soc. 142 (1995) 2631.
[7] T.V. Nguyen, R.E. White, H. Gu, J. Electrochem. Soc. 137 (1990) 2998.
[8] P. Ekdunge, K.V. Rybalka, D. Simonsson, Electrochim. Acta 32 (1987) 659.
[9] P. Ekdunge, D. Simonsson, J. Appl. Electrochem. 19 (1989) 127.
[10] P. Ekdunge, D. Simonsson, J. Appl. Electrochem. 19 (1989) 136.
[11] W.H. Tiedemann, J. Newman, Battery design and optimization princeton, in: S. Gross (Ed.), The Electrochemical Society Soft-bound Proceedings Series, Princeton, NJ, 1979, p. 23.
[12] P.D. Vidts, R.E. White, J. Electrochem. Soc. 144 (1997) 1343.
[13] W.G. Sunu, Electrochemical cell design, in: R.E. White, (Ed.), Plenum, New York, 1984, p. 357.
[14] H.A. Preisig, R.E. White, Computers Chem. Engng. 14 (1990) 179.
[15] D. Fan, R.E. White, J. Electrochem. Soc. 138 (1991) 1688.
[16] H. Bode, Lead–Acid Batteries, R.J. Brodd, Karl V. Kordesch, Translators, Wiley, New York, 1977.
[17] D. Berndt, Maintenance-Free Batteries, 2nd ed., Research Studies Press, Taunton, Somerset, UK, 1997.